Wireless 3 GHz and 30 GHz Vehicle-to-Vehicle Measurements in an Urban Street Scenario

Markus Hofer, David Löschenbrand, Stefan Zelenbaba, Anja Dakić
Benjamin Rainer and Thomas Zemen

Security & Communication Technologies, AIT Austrian Institute of Technology GmbH, Austria
Email: markus.hofer@ait.ac.at

***Abstract*—In this paper we present and discuss results of a wireless vehicle-to-vehicle (V2V) dualband channel measurement campaign at center frequencies of $3.2\,$GHz and $34.3\,$GHz in an urban street scenario. The measurement is conducted using a bandwidth of $155.5\,$MHz and a sounding repetition rate of $62.5\,\mu$s for both bands. At the transmitter side we use omni-directional antennas and at the receiver side directional antennas with 17° opening angles. With this setup, we present the first comparison of simultaneous and dynamic multiband V2V measurements using the time-variant power delay profile (PDP) and the Doppler spectral density (DSD). We find close similarities for the line-of-sight, specular as well as diffuse reflections in both frequency bands, enabling future work for out-of-band beam finding in vehicular mmWave systems.**

***Index Terms*—multiband, mmWave, wireless channel measurements, vehicle-to-vehicle**

I. Introduction

Vehicle-to-vehicle communications will be a key technology for future mobility systems, where fully or semi autonomous vehicles for cargo, public, and personal transport are anticipated to share the streets in a safe and energy-efficient way. Up until recently, mostly communication technologies operating in the sub-6 GHz frequency domain were considered for this purpose, given their technological maturity and cost effectiveness. However, the advance of 5G and 6G increasingly brings also higher frequency bands in the mmWave domain within reach. Wireless propagation characteristics in sub-6 GHz bands are understood and modeled well. Their low isotropic free-space pathloss and little sensitivity to blockage are considered advantageous for vehicle-to-vehicle (V2V) communication. However, increased bandwidth demands as well as the need for radar sensing capabilities call for the application of mmWave communication technologies, despite their comparatively high pathloss and quasi-optic propagation (i.e. little diffraction, small penetration depth).

Consequently, a comparative study of wireless propagation in sub-6 GHz and mmWave bands based on multiband measurements is important for system design as well as the design of frequency diversity transmission architectures. In the latter, critical information is transmitted in a robust low-frequency band, while supplementary data is transmitted in a high-frequency band when it is available; this principle is well known from non-standalone 5G systems [1]. Additionally, the information in one frequency band can be used to help channel estimation and beamforming in the other band [2], [3].

An overview of recent advances and challenges for V2V mmWave communications is given in [4]. The authors underline the small number of available mmWave V2V channel measurements and that most measurements have been conducted in static scenarios.

Static multiband measurements for V2V scenarios are presented in [5]–[8]. In [5] the authors analyze the blockage loss of vehicles and buses at 6.75 GHz, 30 GHz, 60 GHz and 73 GHz for a static V2V scenario. The authors of [6] present simultaneous double-directional ultra-wideband multiband measurements at 6.75 GHz, 33.75 GHz and 60.75 GHz and analyze scattering aspects and large scale parameters in different bands. The work of [8] shows a statistical analysis of V2V measurements at 60 GHz with a bandwidth of 500 MHz for a static scenario with overtaking cars. The results demonstrate that the size of the overtaking vehicle plays a crucial role for the statistics of the vehicular channel during an overtaking maneuver.

Mobile mmWave V2V measurements are shown in [9]–[12]. In [9] a real-time millimeter wave V2V channel sounder is presented using four phased arrays, analyzing the power delay profiles (PDPs) only. In [10] V2V measurements at 60 GHz with a bandwidth of 8 GHz are presented. The results show a PDP with multiple propagation paths but no Doppler spectral density (DSD) is shown. In [11] multiband V2V measurements at 38 GHz and 60 GHz with a bandwidth of 1 GHz and directional horn antennas for transmitter (TX) and receiver (RX) are presented. Contributions from the direct line-of-sight (LOS) and a reflecting metallic guard rail were identified. The work of [12] shows a comparison of sub-6 GHz and mmWave channels for high velocities indoors, where the TX is moving on a rotary arm.

Finally, in [13] vehicle-to-infrastructure (V2I) measurements in centimeter and millimeter bands at 3.2 GHz, 34.3 GHz and 62.35 GHz are presented. The shown results indicate a strong similarity between the respective frequency bands, specifically for specular reflections.

Scientific contribution:

- To the best of our knowledge, we present results of the first *simultaneous* and *dynamic* multiband V2V measure-

ment in an urban scenario with moving TX and RX at center frequencies of 3.2 GHz and 34.3 GHz.
- For both considered bands, we analyze the obtained PDPs and DSDs for similarities and differences and draw conclusions from the results. Our time-variant measurements allow a simultaneous DSD analysis in both bands for the first time.
- The results show that, for the same bandwidth, the propagation conditions between sub-6 GHz and mmWave frequency bands are very similar. Besides specular reflections, also similar diffuse scattering is clearly visible in both bands.

II. Measurement Setup

We perform channel sounding simultaneously at 3.2 GHz and 34.3 GHz to obtain the time-variant channel transfer functions $H_i[m,q]$, where $i \in \{1,2\}$ indicates the frequency band, $m \in \{0,\dots,M-1\}$ denotes the time index and $q \in \{0,\dots,Q-1\}$ denotes the frequency index. We utilize a multitone channel sounding approach. We use a measurement setup similar to [13] with slight modifications. Specifically, we use an Eravant SFA-203403220-KFSF-S1 frequency doubler, a Cernex CBM18403523 power amplifier (PA), an Erzia ERZ-LNA-1600-4000-28-6 low noise amplifier (LNA) and a Marki MMIQ-1037H IQ-mixer. We employ omni-directional antennas at the TX and directional antennas, i.e. a horn and a patch antenna, at the RX. Vertically polarized antennas are used for the measurements. Custom-built omni-directional monopole antennas are utilized as TX antennas. They are mounted on the rooftop of the TX car as shown in Fig. 1. For 34.3 GHz a $\lambda/4$ monopole antenna with a rectangular metallic ground plane is used. The ground plane size is about $14\,\lambda$. At 3.2 GHz a $\lambda/4$ monopole antenna with radials is used to attain a comparable pattern at reduced size.

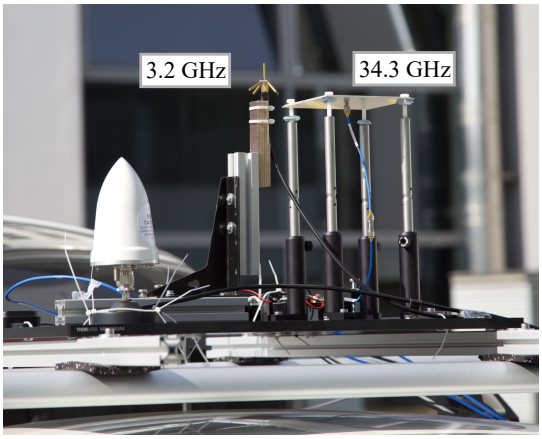

Fig. 1. Transmit antennas mounted on the rooftop of the TX car.

The directional RX antennas are mounted on the rooftop of the RX car as shown in Fig. 2. For 3.2 GHz, a patch array antenna with 17° horizontal half power beam width (HPBW) and 18 dBi gain is used. For 34.3 GHz, a Pasternack PE9850B/2F-20 standard gain horn antenna with 16.7° horizontal HPBW and 20 dBi gain is utilized.

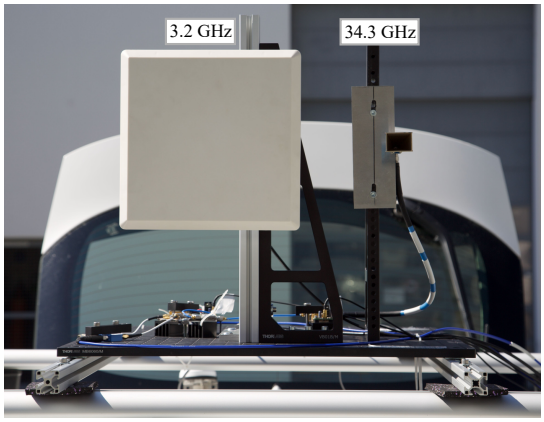

Fig. 2. Receive antennas mounted on the rooftop of the RX car.

A. Sounding Signal

A complex baseband multitone signal is used to measure the time-variant channel characteristics [13]–[15]. The multitone signal consists of $Q = 311$ subcarriers. We choose a subcarrier spacing of $\Delta f = 1/T = 500\,\text{kHz}$, with T the period of the sounding signal, such that we achieve a maximum excess delay of $\tau_{\text{max}} = 2\,\mu\text{s}$. Hence, the effective sounding bandwidth is $B = Q\Delta f = 155.5\,\text{MHz}$.

We use the method of [16] to obtain a multitone signal with a crest factor of 1.25 (see [14] for more details). The sounding signal is constructed by concatenating five repetitions of the multitone signal. This leads to a total sounding signal length of $5\,T = 10\,\mu\text{s}$. We use the first period T of the sounding signal as cyclic prefix (CP) (see [13]–[15] for more details).

At the RX, the sounding signal is sampled and stored. The frequency domain signal at the RX is obtained by a discrete fast Fourier transform (FFT). Two repetitions of the multitone signal are used to obtain an oversampled frequency domain signal. Since the sounding signal is known at the RX, the calibrated channel transfer function is obtained by dividing the received sounding signal in the frequency domain by the known sounding signal for every second subcarrier, i.e., [14]

$$\hat{H}_i[q] = \frac{Y_i[q]}{X_i[q]\hat{H}_i^{\text{RF}}[q]}. \tag{1}$$

Here, $\hat{H}_i^{\text{RF}}[q]$ is the calibration transfer function of the i-th radio frequency (RF) chain, q is the subcarrier index, $X_i[q]$ are the known complex weights of the sounding signal at the different subcarriers and $Y_i[q]$ are the complex weights of the subcarriers after downsampling. The calibration function is obtained by connecting TX with RX directly via attenuators and measuring the transfer function. For a better signal-to-noise ratio (SNR) of the calibration transfer function estimation, it is averaged over 64 repetitions.

For both frequency bands, the same measurement principle is used. The sounding is performed at regular time intervals of $T_{\text{R}} = 62.5\,\mu\text{s}$. This allows a Doppler estimation up to a

relative velocity of $v_{\max} = {c_0 f_{\mathrm{Dmax}}}/{f_\mathrm{c}} = {c_0}/{2T_\mathrm{R} f_\mathrm{c}} = 69.97\,\mathrm{m/s}$, where c_0 is the speed of light in air, f_c is the carrier frequency of the highest frequency band, and $f_{\mathrm{Dmax}} = 1/(2T_\mathrm{R})$.

B. Synchronization

At TX and RX, Precision Test Systems GPS10eR [17] Rubidium clocks provide a 10 MHz reference signal with low phase noise and a pulse per second (PPS) signal for timing synchronization between TX and RX. Before the measurement starts, the RX Rubidium clock is connected via coaxial cables to the TX Rubidium clock and synchronized to it. The TX Rubidium clock acts as primary clock source.

III. Scenario Description

We conduct channel measurements for a V2V scenario in an urban street environment as depicted in Fig. 3. Moving TX and RX cars pass each other on a two-lane two-way street, with office buildings on both sides of the road, a factory with a large metallic surface on the west end and trees on the roadside. Ten repetitions are performed for the measurement. The duration of one measurement run is 30 s.

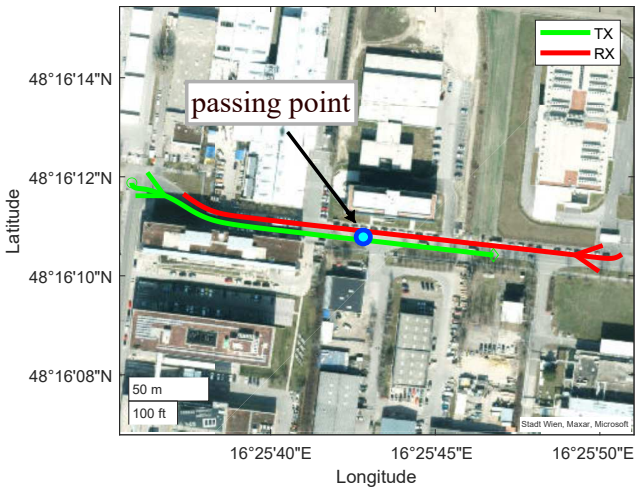

Fig. 3. TX and RX pass each other at the indicated passing point.

IV. Measurement Evaluation

A. Local Scattering Function

We use the local scattering function (LSF) [13], [18], [19] and its marginals for measurement data evaluation. With the time-variant frequency response $H_i[m,q]$, the estimate of the LSF is given by

$$\hat{\mathcal{C}}_i[k_\mathrm{t};n,p] = \frac{1}{IJ}\sum_{w=0}^{IJ-1}\left|\mathcal{H}_i^{(G_w)}[k_\mathrm{t};n,p]\right|^2, \tag{2}$$

with the Doppler index $p \in \{-M/2\ldots, M/2-1\}$, the delay index $n \in \{0,\ldots,Q-1\}$ and the stationarity region index k_t. The delay and Doppler shift resolution are defined by $\tau_\mathrm{s} = {1}/{Q\Delta f}$ and $\nu_\mathrm{s} = {1}/{MT_\mathrm{R}}$. The tapered frequency response is

$$\mathcal{H}_i^{(G_w)}[k_\mathrm{t};n,p] = \sum_{m=-M/2}^{M/2-1}\sum_{q=-(Q-1)/2}^{(Q-1)/2} H_i[m+Mk_\mathrm{t},q] \cdot G_w[m,q]\mathrm{e}^{-\mathrm{j}2\pi(pm-nq)}, \tag{3}$$

where the tapers $G_w[m,q]$ are two-dimensional discrete prolate spheroidal (DPS) sequences as shown in detail in [18], [20]. The number of tapers in the time and frequency domain is set to $I=2$ and $J=1$, respectively [8], [18].

We choose $M=1600$, which corresponds to an observation duration of 100 ms. For a velocity of $v = 50\,\mathrm{km/h}$ ($= 13.89\,\mathrm{m/s}$), this corresponds to a calculation of the LSF over a spatial window of approximately $14.81\,\lambda_1$ for 3.2 GHz and $158.8\,\lambda_2$ for 34.3 GHz with λ_i, $i \in \{1,2\}$ being the wavelengths of the two frequency bands.

We calculate the PDP and DSD as marginals of the LSF over the Doppler domain or the delay domain, respectively:

$$\hat{\mathcal{P}}_{\tau,i}[k_\mathrm{t};n] = E_p\left\{\hat{\mathcal{C}}_i[k_\mathrm{t};n,p]\right\} = \frac{1}{M}\sum_{p=-M/2}^{M/2-1}\hat{\mathcal{C}}_i[k_\mathrm{t};n,p], \tag{4}$$

$$\hat{\mathcal{P}}_{\nu,i}[k_\mathrm{t};p] = E_n\left\{\hat{\mathcal{C}}_i[k_\mathrm{t};n,p]\right\} = \frac{1}{Q}\sum_{n=0}^{Q-1}\hat{\mathcal{C}}_i[k_\mathrm{t};n,p]. \tag{5}$$

We normalize the Doppler shifts of the DSDs to their respective wavelength and thus obtain normalized Doppler shifts or velocities

$$v_i = f_{\mathrm{D},i}\lambda_i, \tag{6}$$

to allow for a better comparability between different frequency bands.

V. Result Analysis

A. Comparison of PDPs and DSDs

We normalize the power of the PDPs and DSDs by their respective maxima within their frequency band, i.e., for each frequency band we calculate $\hat{\mathcal{P}}_\tau^\mathrm{N}[k_\mathrm{t};n] = \hat{\mathcal{P}}_\tau[k_\mathrm{t};n]/\max_{k_\mathrm{t};n}(\hat{\mathcal{P}}_\tau[k_\mathrm{t};n])$ and $\hat{\mathcal{P}}_\nu^\mathrm{N}[k_\mathrm{t};n] = \hat{\mathcal{P}}_\nu[k_\mathrm{t};n]/\max_{k_\mathrm{t};n}(\hat{\mathcal{P}}_\nu[k_\mathrm{t};n])$. We choose the displayed dynamic range to be 45 dB in each band.

In Fig. 4 and Fig. 5, the PDP and DSD at 3.2 GHz and 34.3 GHz are shown. A clear LOS path is visible until around second 20, where TX passes RX and moves out of the main lobe of the RX antennas, leading to a significant power drop. Comparing the PDPs, one can clearly observe the similarities between the bands. Specular scatteres are visible in both bands. Diffuse scattering can be noticed in both bands from second 12, furthermore some static discrete (SD) scatteres are visible. The approximately constant delay at around 1 μs originates from a large metallic surface placed on the side of a manufacturing hall. This leads to the hypothesis that, similar to the sub-6 GHz band, diffuse scattering will contribute to an increase of the delay spread in mmWave bands. Furthermore, the general shapes of the DSDs match, too.

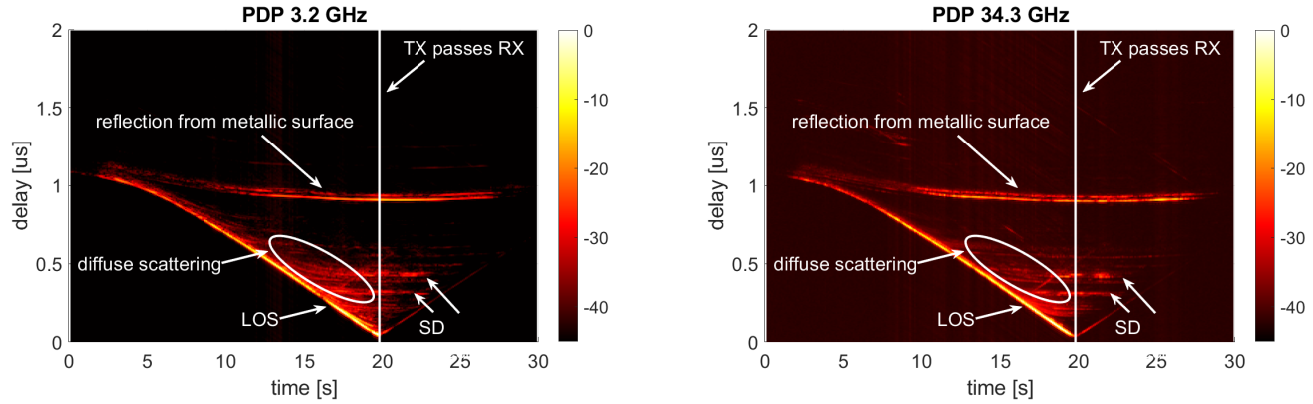

(a) PDP vs. time for 3.2 GHz. (b) PDP vs. time for 34.3 GHz.

Fig. 4. PDPs of passing scenario for (left) the 3.2 GHz band and (right) the 34.3 GHz band. The max. power is normalized to 0 dB.

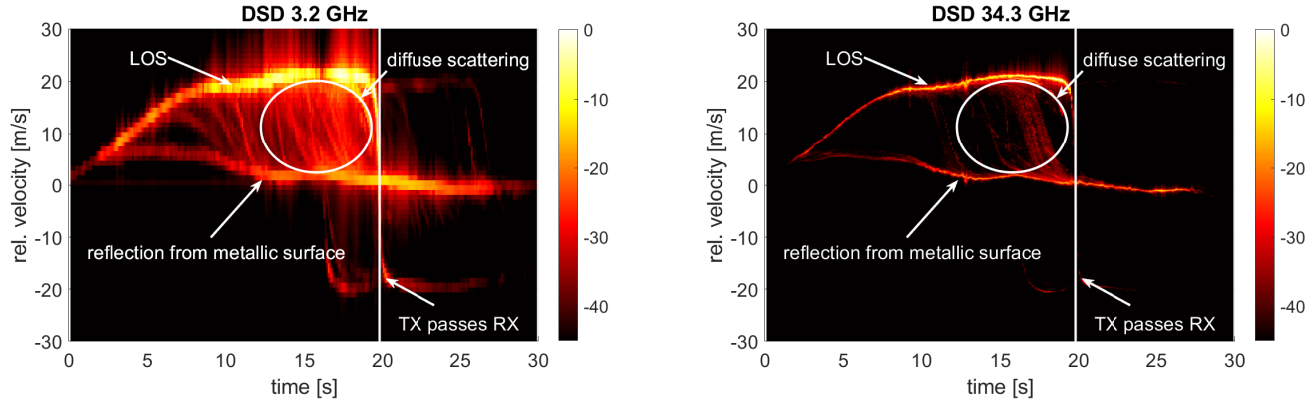

(a) DSD vs. time for 3.2 GHz. (b) DSD vs. time for 34.3 GHz.

Fig. 5. DSDs of passing scenario for (left) the 3.2 GHz band and (right) the 34.3 GHz band. The max. power is normalized to 0 dB, the Doppler shift axis rescaled to relative velocity.

B. Correlation between the PDPs

In Fig. 6 we show the empirical cumulative distribution function (CDF) of the correlation between the PDPs of the 3.2 GHz band and the 34.3 GHz band of the 10 measurement runs. We calculate the Pearson correlation coefficient according to

$$\rho_{i,j}[k_\mathrm{t}] = \frac{C_{i,j}[k_\mathrm{t}]}{\sigma_i[k_\mathrm{t}]\sigma_j[k_\mathrm{t}]}, \tag{7}$$

where

$$C_{i,j}[k_\mathrm{t}] = \frac{1}{Q}\sum_{n=0}^{Q-1}\left(\hat{\mathcal{P}}_{\tau,i}[k_\mathrm{t};n] - \mu_{\tau,i}[k_\mathrm{t}]\right) \left(\hat{\mathcal{P}}_{\tau,j}[k_\mathrm{t};n] - \mu_{\tau,j}[k_\mathrm{t}]\right)^*, \tag{8}$$

with

$$\sigma_i[k_\mathrm{t}]^2 = \frac{1}{Q}\sum_{n=0}^{Q-1}|\hat{\mathcal{P}}_{\tau,i}[k_\mathrm{t};n] - \mu_{\tau,i}[k_\mathrm{t}]|^2 \tag{9}$$

and

$$\mu_{\tau,i}[k_\mathrm{t}] = \frac{1}{Q}\sum_{n=0}^{Q-1}\hat{\mathcal{P}}_{\tau,i}[k_\mathrm{t};n] \tag{10}$$

where $i \neq j$.

We observe CDFs with similar characteristics over measurement runs, although the probability for high correlation (above 0.8) varies by almost 30 % between measurement runs. The correlation between 3 and 30 GHz is higher than 0.9 for 30 % to 50 % of the measurement time, while the correlation is higher than 0.5 for 70 % to 90 % of the measurement time, depending on the realization of the measurement run.

VI. Conclusion

In this paper, we present the first simultaneous and dynamic multiband V2V measurements for an urban street scenario. The results show strong similarities between the PDPs and DSDs of both bands, specifically specular reflections are present in both bands. Furthermore, it was observed that diffuse scatterers are clearly visible in the mmWave band, thus disproving the assumption of a sparse multipath component distribution in that frequency range. The multipath components were found to be similarly distributed in the sub-6 GHz and mmWave band. The strong similarity of specular and diffuse reflections in the PDP and DSD in both bands provide a strong motivation to further explore the use of 3.2 GHz channel properties for beamforming at 34.3 GHz.

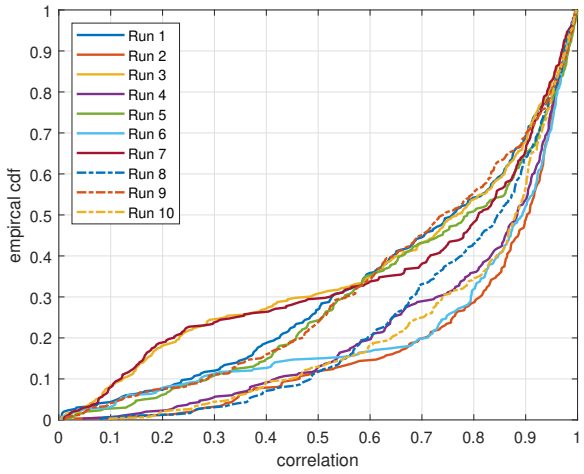

Fig. 6. Empirical correlation between the PDPs of the 3.2 GHz and the 34.3 GHz band for an urban street scenario for 10 measurement runs.

ACKNOWLEDGMENT

This work was funded within the project DEDICATE (Principal Scientist grant) at the AIT Austrian Institute of Technology.

REFERENCES

[1] E. Dahlman, S. Parkvall, and J. Skold, *5G NR: The next generation wireless access technology*. Academic Press, 2020.

[2] A. Ali, N. González-Prelcic, and R. W. Heath, "Millimeter wave beam-selection using out-of-band spatial information," *IEEE Transactions on Wireless Communications*, vol. 17, no. 2, pp. 1038–1052, 2017.

[3] D. Burghal, R. Wang, and A. F. Molisch, "Band assignment in dual band systems: A learning-based approach," in *MILCOM 2018-2018 IEEE Military Communications Conference (MILCOM)*. IEEE, 2018, pp. 7–13.

[4] R. He, C. Schneider, B. Ai, G. Wang, Z. Zhong, D. A. Dupleich, R. S. Thomae, M. Boban, J. Luo, and Y. Zhang, "Propagation channels of 5G millimeter-wave vehicle-to-vehicle communications: Recent advances and future challenges," *IEEE Vehicular Technology Magazine*, vol. 15, no. 1, pp. 16–26, 2020.

[5] M. Boban, D. Dupleich, N. Iqbal, J. Luo, C. Schneider, R. Müller, Z. Yu, D. Steer, T. Jämsä, J. Li, and R. S. Thomä, "Multi-band vehicle-to-vehicle channel characterization in the presence of vehicle blockage," *IEEE Access*, vol. 7, pp. 9724–9735, 2019.

[6] D. Dupleich, R. Müller, M. Landmann, E. Shinwasusin, K. Saito, J. Takada, J. Luo, R. Thomä, and G. Del Galdo, "Multi-band propagation and radio channel characterization in street canyon scenarios for 5G and beyond," *IEEE Access*, vol. 7, pp. 160 385–160 396, 2019.

[7] D. Dupleich, R. Müller, C. Schneider, S. Skoblikov, J. Luo, M. Boban, G. Del Galdo, and R. Thomä, "Multi-band vehicle to vehicle channel measurements from 6 GHz to 60 GHz at "T" intersection," in *2019 IEEE 2nd Connected and Automated Vehicles Symposium (CAVS)*, 2019, pp. 1–5.

[8] E. Zöchmann, M. Hofer, M. Lerch, S. Pratschner, L. Bernadó, J. Blumenstein, S. Caban, S. Sangodoyin, H. Groll, T. Zemen, A. Prokeš, M. Rupp, A. F. Molisch, and C. F. Mecklenbräuker, "Position-specific statistics of 60 GHz vehicular channels during overtaking," *IEEE Access*, vol. 7, pp. 14 216–14 232, 2019.

[9] A. Chopra, A. Thornburg, O. Kanhere, S. S. Ghassemzadeh, M. Majmundar, and T. S. Rappaport, "A real-time millimeter wave V2V channel sounder," pp. 1–6, Apr. 2022. [Online]. Available: https://arxiv.org/abs/2203.09057

[10] A. Prokes, J. Vychodil, T. Mikulasek, J. Blumenstein, E. Zöchmann, H. Groll, C. F. Mecklenbräuker, M. Hofer, D. Löschenbrand, L. Bernadó, T. Zemen, S. Sangodoyin, and A. Molisch, "Time-domain broadband 60 GHz channel sounder for vehicle-to-vehicle channel measurement," in *2018 IEEE Vehicular Networking Conference (VNC)*, 2018, pp. 1–7.

[11] M. García Sánchez, M. Portela Táboas, and E. Lemos Cid, "Millimeter wave radio channel characterization for 5G vehicle-to-vehicle communications," *Measurement*, vol. 95, pp. 223–229, 2017. [Online]. Available: https://www.sciencedirect.com/science/article/pii/S0263224116305668

[12] F. Pasic, S. Pratschner, R. Langwieser, D. Schuetzenhoefer, E. Jirousek, H. Groll, S. Caban, and M. Rupp, "Sub 6 GHz versus mmWave measurements in a controlled high-mobility environment," in *WSA 2021; 25th International ITG Workshop on Smart Antennas*, 2021, pp. 1–4.

[13] M. Hofer, D. Löschenbrand, J. Blumenstein, H. Groll, S. Zelenbaba, B. Rainer, L. Bernadó, J. Vychodil, T. Mikulasek, E. Zöchmann, S. Sangodoyin, H. Hammoud, B. Schrenk, R. Langwieser, S. Pratschner, A. Prokes, A. F. Molisch, C. F. Mecklenbräuker, and T. Zemen, "Wireless vehicular multiband measurements in centimeterwave and millimeterwave bands," in *2021 IEEE 32nd Annual International Symposium on Personal, Indoor and Mobile Radio Communications (PIMRC)*, 2021, pp. 836–841.

[14] D. Löschenbrand, M. Hofer, L. Bernadó, G. Humer, B. Schrenk, S. Zelenbaba, and T. Zemen, "Distributed massive MIMO channel measurements in urban vehicular scenario," in *2019 13th European Conference on Antennas and Propagation (EuCAP)*, 2019, pp. 1–5.

[15] S. Zelenbaba, M. Hofer, D. Löschenbrand, G. Kail, M. Schiefer, and T. Zemen, "Spatial properties of industrial wireless ultra-reliable low-latency communication MIMO links," in *2019 53rd Asilomar Conference on Signals, Systems, and Computers*, 2019, pp. 1054–1058.

[16] M. Friese, "Multitone signals with low crest factor," *IEEE Transactions on Communications*, vol. 45, no. 10, pp. 1338–1344, 1997.

[17] Accessed: 2022-06-30. [Online]. Available: https://www.ptsyst.com/

[18] L. Bernadó, T. Zemen, F. Tufvesson, A. F. Molisch, and C. F. Mecklenbrauker, "Delay and Doppler spreads of nonstationary vehicular channels for safety-relevant scenarios," *IEEE Trans. Veh. Technol.*, vol. 63, no. 1, pp. 82–93, Jan. 2014.

[19] G. Matz, "On non-wssus wireless fading channels," *IEEE Trans. Wireless Commun.*, vol. 4, no. 5, pp. 2465–2478, Sep. 2005.

[20] D. Slepian, "Prolate spheroidal wave functions, Fourier analysis, and uncertainty-V: The discrete case," *Bell Syst. Techn J.*, vol. 57, no. 5, pp. 1371–1430, May 1978.